Atomic number and crystallographic contrast images with the SEM: a review of backscattered electron techniques

GEOFFREY E. LLOYD

Department of Earth Sciences, The University, Leeds LS2 9JT

Abstract

Backscattered electrons (BSE) are incident electrons reflected back from a target specimen and imaged with the scanning electron microscope (SEM). Three distinct BSE signals exist: atomic number or Z-contrast, in which composition determines image contrast; orientation contrast, in which specimen crystal structure determines image contrast; and electron channelling patterns (ECP), which are unique for a particular crystal orientation. The origins of these three signals are described, with particular attention being given to the necessary SEM operational and specimen preparation requirements. Z-contrast images are relatively simple to obtain and also have a familiar appearance such that their usage should become commonplace. ECP in comparison require subsequent interpretation which depends on the crystal structure and the relationship between crystal and specimen coordinate systems. A general solution to ECP interpretation is therefore presented, involving the construction of reference 'ECP-maps' over the surface of a sphere. A brief summary of the applications and potential use of the three BSE signals in the geological sciences is also given.

KEYWORDS: contrast images, scanning electron microscopy, backscattered electrons.

Introduction: scanning electron microscopy

THE electron-optical lens system of any scanning electron microscope (SEM) acts to focus a beam of electrons emitted from an electron gun into a fine probe which impinges on the surface of a target specimen, where electron–specimen interactions result in a number of distinct emission signals from which images can be derived (see for example Oatley, 1972; Wells, 1974; Goldstein and Yakowitz, 1975; Goldstein et al., 1981). The probe current, and hence the strengths of the various emission signals, is determined by the electron source and condenser lens system, whereas the probe diameter, and hence the spatial resolution, is largely determined by the gun geometry and objective lens. In practice, improved resolution is generally only possible at the expense of probe current and consequently maximum probe current is limited for a given probe size. The different emission signals result from electrostatic interactions between the probe or incident or primary electrons and the target specimen, but some of these interactions are inelastic (e.g. secondary electron emission) whereas others are elastic (e.g. backscattered electon emission).

Each signal originates from a specific emission volume within the target specimen, the size of which depends on the penetration depths of the probe electrons and hence on probe energy (i.e. accelerating voltage), probe diameter and the morphology, composition and crystal structure of the target. As the probe penetrates the target, the electrons diverge, resulting in a reduction in resolution and also in the strength of the emission signal. The energy spectrum of the emitted electrons therefore consists of three distinct regions: (I) elastically scattered electrons with energies similar to those of the probe electrons (E_0); (II) multiply scattered electrons with energies in the range 50 eV to E_0; and (III) low-energy electrons (i.e. < 50 eV). Secondary electrons (SE) occupy Group III, whilst backscattered electrons (BSE) should in principle comprise Group I, but due to slight inelastic effects a significant proportion of Group II electrons are also emitted as BSE.

Conventional scanning electron microscopy makes use of the SE emission characteristics of rough surfaces to produce images based on specimen surface topography. SE images can be obtained at magnifications very much higher than
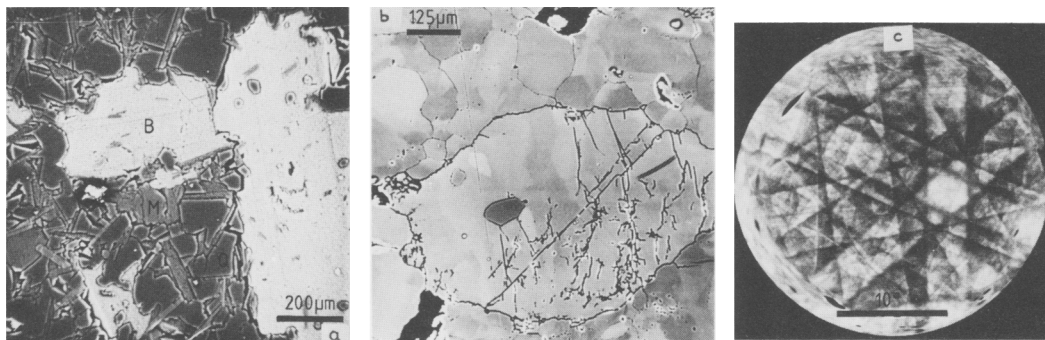
FIG. 1. Examples of different types of SEM/BSE image. All specimens carbon-coated and imaged at 30 kV accelerating voltage. (*a*) Atomic number or *Z*-contrast image of a hornfelsed metagreywacke; minerals present are (in increasing order of brightness) quartz (Q), muscovite (M), and biotite (B). (*b*) Orientation or crystallographic contrast image of grain and subgrain microstructure in feldspar (porphyroclast) and quartz (matrix). (*c*) Electron channelling pattern image from an individual pyrite grain; the centre of the pattern has an orientation close to {114}.

those possible with the optical microscope, whilst the incorporation of suitable X-ray microanalytical facilities (either energy- or wavelength-dispersive systems) makes simultaneous compositional determination routinely possible. These attributes have made the SEM a popular instrument in geological research for many years. However, the existence of images based on the emission of backscattered primary electrons has largely been ignored by geologists. BSE originate from within the target specimen and are capable of providing images based on composition and crystal structure (e.g. Fig. 1). The properties of BSE therefore differ considerably from those of SE and this is reflected in the need for separate electron detection systems, specimen preparation and image interpretation. This review of BSE techniques considers each of these aspects in turn, as well as discussing possible applications in the Earth Sciences.

Emission and detection of backscattered electrons

BSE emission

BSE are primary electrons which have been reflected back from a target specimen by elastic scattering events in one of two ways (e.g. Niedrig, 1978): (1) the strong Coulomb field of an atomic nucleus can cause a single large (> 90°) deflection in the trajectory of an incident electron (i.e. Rutherford scattering); (2) incident electrons can undergo multiple low-angle deflections which together comprise a deflection of > 90°. Both types of scattering event result in BSE with energies somewhat less than the incident beam and hence there must also be some minor inelastic scattering involved (usually associated with the emission of white X-radiation).

The shape of the interaction volume between incident electrons and target specimen was qualitatively predicted by Duncumb and Shields (1963): for the same beam energy electrons penetrate more deeply into materials with low atomic number (*Z*) and the electron distribution tends towards pear-shaped; increasing energy serves only to increase the electron path-length such that the envelope expands but retains the same shape. Recently, it has been possible to predict the shape of this volume more accurately by direct observation of plastic materials which undergo chemical changes under electron bombardment, and indirectly by the Monte Carlo simulation technique (see Goldstein *et al.*, 1981, pp. 56–68). These approaches show that in low *Z* materials the interaction volume has dimensions of several micrometres and depth > width, resulting in distinct pear-shapes. This shape can be explained by inelastic scattering events being more important at low *Z* and consequently electrons are able to penetrate without significant scattering. But, as the electrons lose energy, elastic scattering becomes more important and deviations increase to produce the bulbous region. As *Z* increases, electron path-lengths decrease because elastic scattering becomes more significant and scattering angles therefore increase such that electron trajectories deviate quickly from beam-parallel to produce an interaction volume with an approximately spherical shape. It is also clear from Monte Carlo simulations that the interaction volume has a diffuse rather than sharp boundary, and that electron energies are highest at the point of beam incidence.

The fraction of incident electrons which reappear as BSE (known as the BSE coefficient η) increases

with specimen atomic number and this is consistent with elastic scattering events occurring closer to the specimen surface. As Z increases, the energy of the BSE also increases towards the incident beam energy, E_0 (Heinrich, 1966; Bishop, 1966). There appears to be little dependence of η on probe current or accelerating voltage; a slight decrease is observed as voltage increases, whilst a tendency for η to decrease somewhat at lower voltages for heavier elements has also been observed (Heinrich, 1966). The changes in interaction volume described above largely determine the spatial resolution of any BSE signal image since the divergence (scattering) of the incident electrons increases with volume such that the actual surface area from which BSE emission occurs also increases (Shimuzu and Murata, 1971). Thus, as volume decreases with increasing Z, targets with high Z should provide better spatial resolution (Cosslett and Thomas, 1965). However, although BSE spatial resolution is generally better than X-ray resolution, it is significantly inferior to SE spatial resolution since the emission of SE occurs from a much smaller, near-surface volume (Fig. 2). Furthermore, the cross-section of emission intensity of SE is Gaussian and has a much better signal-to-noise ratio than BSE emission, which for normal incidence has a spherical cross-section.

Emission of BSE is highly directional and becomes more so as the angle of tilt of the target relative to the incident beam moves away from normal incidence. This is because the beam strikes the target at shallower angles, which reduces both electron penetration and scattering angles. Wells (1970) has suggested that this reduction in penetration and scattering should lead to improved BSE spatial resolution. However, rough specimens also effectively produce a large variation in tilt angles such that BSE emission can vary significantly from point to point on the surface. This means that BSE emission due to other specimen characteristics (see below) may be suppressed. It therefore follows that the best BSE images are obtained from specimen surfaces which have been polished flat and hence that specimen preparation forms a significant part of any SEM/BSE investigation (see below).

BSE detection

The Everhart-Thornley detector system (Everhart and Thornley, 1960) used in most SEM to collect secondary electrons is less suitable for BSE detection due to the directionality and higher energies of BSE. Any BSE detector must therefore be positioned geometrically to subtend as large a solid angle as possible of the BSE emission distribution, which has a cosine form (e.g. Wells, 1974, pp. 52–60). In practice it is most convenient to use

normal beam incidence, in which case the optimum detector position is vertically above the target. The electron beam strikes the target by passing through a small hole in the detector.
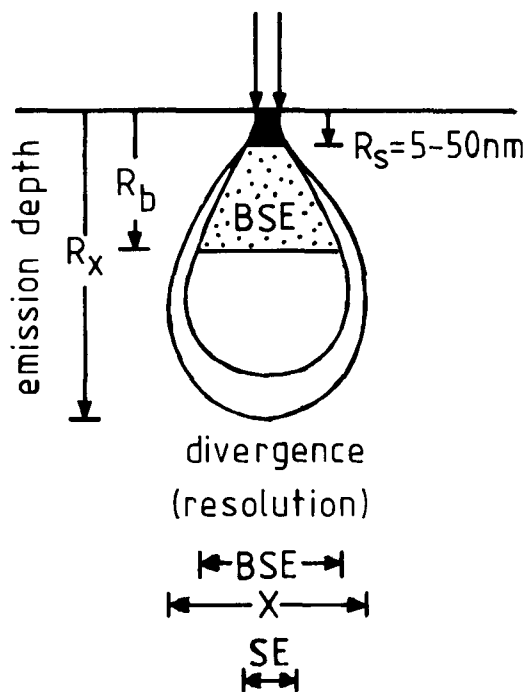

FIG. 2. Comparison of penetration ranges (R_s, R_b, R_x) and spatial resolutions (SE, BSE, X) for secondary electron, backscattered electron and X-ray emission signals from elements with low to medium atomic numbers. After Goldstein and Yakowitz (1975).

Two types of BSE detector are currently available, the scintillator–photomultiplier detector (Wells, 1970; Robinson, 1973 and 1975; Schur et al., 1974) and the solid-state detector (Wolf and Everhart, 1969; Lin and Becker, 1975; Stephen et al., 1975). The relative merits of the two systems have been discussed by Robinson and Nickel (1983) and Hall and Lloyd (1983). My own experience has led me to prefer the solid-state variety, particularly because they are slim and clamp simply on to the roof of the SEM specimen chamber which allows operation at short (i.e. ~ 5 mm) working distances. As we shall see, short working distances are important for electron channelling analysis.

BSE image formation

The formation of any BSE image on the SEM cathode ray tube (CRT) is identical to all other

SEM images; the CRT is scanned in synchronism with the passage of the electron beam over the target specimen such that a one-to-one correspondence exists between each point on the specimen and each component (pixel) of the screen. The intensity of the image at each pixel is determined by the number of electrons emitted from the corresponding point on the target, whilst image contrast is simply the difference in intensity from pixel to pixel. The quality of the actual image depends on the amount of 'noise' present. Noise is mainly introduced either during signal emission at the target or during signal amplification, and the noise level can usually be reduced by increasing the emission signal and/or decreasing the scanning rate of the electron beam. However, image noise may ultimately determine the maximum possible BSE contrast resolution.

Due to the way BSE signal is transmitted from target to CRT it is possible to preferentially treat useful components of the total signal at the expense of the rest. Several different types of 'signal processing' are available within the standard configuration of an SEM (Wells, 1974; Newbury, 1975): black-level correction (D.C. suppression), intensity modulation (gamma correction), image differentiation and y-modulation. Of these, black-level correction is perhaps most useful in BSE images because it allows the background to the total signal to be subtracted with a concomitant amplification of the remainder. Similar effects may be achieved via gamma correction.

Backscattered electron signals

Atomic number or Z contrast

Atomic number or Z-contrast (e.g. Fig. 1a) is the most easily obtainable BSE image. It arises from the dependence of the BSE emission coefficient (η) on target atomic number (Z). In specimens consisting of only a single phase, Z and hence η are constant and the BSE atomic number image therefore consists of a uniform intensity with no contrast. However, in polyphase specimens Z and hence η vary from phase to phase such that the BSE image contains different intensities and contrasts, with higher Z phases appearing brighter (Fig. 3a). SE images of the same area (Fig. 3b) contain less detail (especially when the specimen surface has been polished flat) because SE emission is largely independent of Z. In rough specimens the directional characteristics of BSE emission can be used to provide topographic images but this roughness will degrade any Z-contrast image. The performance of any BSE system in examining topographic specimens ultimately depends on the difference in Z between component phases. In general, surface topography should be avoided and all specimens should be polished flat.
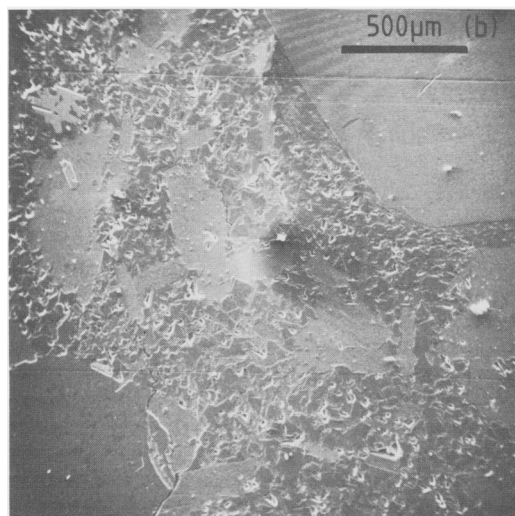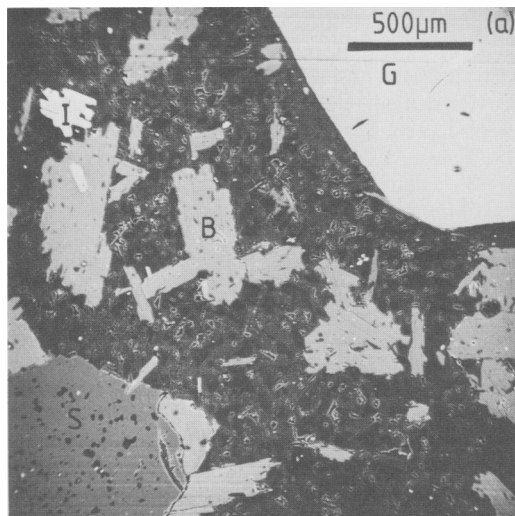

FIG. 3. (a) Example of backscattered electron Z-contrast image: hornfelsed metagreywacke, with the following minerals present (in increasing order of brightness): equant quartz and prismatic muscovite forming the matrix (see Fig. 1a for detail), porphyroblastic staurolite (S), biotite (B) and garnet (G), and matrix ilmenite (I). Compare the contrasts shown with those predicted by equation 2 or inferred in Fig. 4b. (b) Same area imaged using secondary electrons; note the considerably lower Z-contrast effect and also the suppression of topographic contrast due to using a specimen which had been polished flat. Both imaged at 30 kV; specimen carbon-coated.

The relationship between Z and η has been determined experimentally for the pure elements (Heinrich, 1964; Bishop, 1966 and 1974),

$$\eta = \frac{\ln Z}{6} - \frac{1}{4} \quad (Z \geqslant 10). \tag{1}$$

However, most minerals are not pure elements and many have complex compositions. In such cases it is necessary to amend eqn. (1) by defining a weighted mean BSE coefficient (Heinrich, 1966),

$$\bar{\eta} = \sum_{i=1}^{n} C_i \eta_i \tag{2}$$

where C_i is the concentration by weight of each element in the composition, η_i is the elemental BSE coefficient and n is the number of elements present. To observe actual detail in a Z-contrast image some difference in Z must be present. For two minerals A and B this contrast is generally defined,

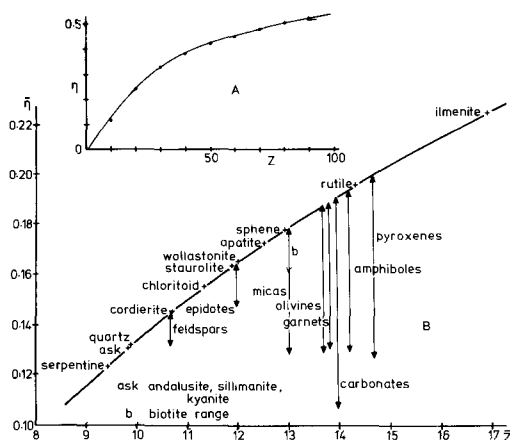$$\delta = \frac{\text{signal (max)} - \text{signal (min)}}{\text{signal (max)}}. \tag{3}$$

FIG. 4. Relationship between BSE coefficient (η or $\bar{\eta}$) and atomic number (Z or $\bar{Z}$). (A) Pure elements (after Bishop, 1966 and Heinrich, 1964). (B) Major rock-forming minerals (after Hall and Lloyd, 1981). The values of $\bar{\eta}$ and $\bar{Z}$ were determined using the most general formula available for each mineral and the BASIC computer program 'MEATNO'. Note that variations in composition (e.g. amphiboles etc.) lead to a range of $\bar{Z}$ values and hence a range of $\bar{\eta}$ values which in turn causes variations in image contrast.

Equations 1 and 2 are shown graphically in Fig. 4 for the pure elements and some common rock-forming minerals. The values of $\bar{\eta}$ and $\bar{Z}$ (the mean

atomic number) were derived using a BASIC computer program 'MEATNO'* in which

$$\bar{Z} = \frac{\Sigma(NAZ)}{\Sigma(NA)} \tag{4}$$

where N is the number of atoms of each element with atomic weight A and atomic number Z (ΣNA is the molecular weight). Note that minerals which belong to solid-solution series (e.g. amphiboles, pyroxenes, etc.) have a range of compositions which yield different $\bar{Z}$ and $\bar{\eta}$ values, and hence Z-contrast images of varying intensities.

From Fig. 4 it is apparent that for most minerals the amount of Z-contrast signal available is only a small proportion of that theoretically possible (typically $< 20\%$) and thus from eqn. (3) any observed contrasts will be generally slight. It is therefore usually necessary to employ some/considerable black-level backing-off in Z-contrast images. Indeed, in many instances it may even be necessary to expand the contrast in a small part of the image at the expense of detail elsewhere. Hall and Lloyd (1981) were able to detect contrasts equivalent to compositional differences of $0.1Z$, but recent developments in BSE detector systems and signal amplification have improved this figure to $0.01Z$. However, Z-contrast resolution can be degraded by the presence of adjacent mineral phases due to the penetration and divergence of the incident beam which means that the BSE can originate from different phases (see Fig. 5). This effect can also lead to a decrease in the overall image resolution since the mineral boundaries become blurred, especially at high magnifications. It should be possible to improve resolution by using lower accelerating voltages; the weaker emission signal being compensated for by new detectors with improved performances. In fact, preliminary experience suggests that with the detectors available in 1986, $\sim 10\,\text{keV}$ produces optimum contrast and resolution up to at least $10\,000$ times normal magnification.

Electron channelling

Although most of the total BSE signal is due to Z-contrast effects, in crystalline materials a contribution is also made from the interaction between primary electrons and the crystal structure of the target. This is known as electron channelling (EC) and occurs because the range of primary electrons in the target (typically up to $\sim 500\,\text{nm}$) is considerably greater than any periodic arrangement of atoms in a crystal structure, such that the electrons are 'channelled' between the rows of atoms (e.g.

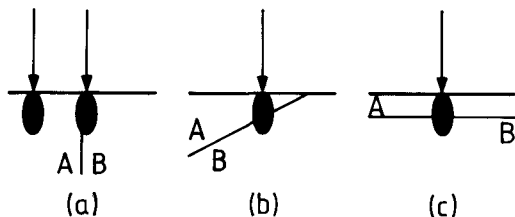* The computer program MEATNO is given in Appendix 1.

FIG. 5. Effect of grain or phase boundary on Z-contrast images and resolutions. (a) Electron beam incident on phase A interacts only with this phase on penetration, whereas beam incident on phase B expands to interact with both A and B, resulting in an image contrast which is some function of ($\bar{\eta}_A$, $\bar{\eta}_B$). Sometimes an electron interaction occurs which yields excess BSE, producing a 'haloed' grain boundary. (b) Gently sloping phase boundary means that an electron beam apparently incident only on phase A actually penetrates to interact with phase B, resulting in an image contrast which is some function of ($\bar{\eta}_A$, $\bar{\eta}_B$). This effect is generally easy to recognize as there is a gradational contrast change in phase A but a sharp change in phase B, although it may be misinterpreted as a diffusion effect. (c) Thin phase A means that the electron beam penetrates through to interact with an unobserved phase B; image contrast is again some function ($\bar{\eta}_A$, $\bar{\eta}_B$). This represents a major problem, although it can be overcome somewhat if polished thin-sections are used and monitored optically. Working at low accelerating voltages may also provide a solution, since these reduce electron penetration.

Hirsch et al., 1962). However, whereas for some angles of beam incidence the atomic packing density is relatively high and the electrons tend to interact with the crystal structure close to the surface (Fig. 6a), for other angles of incidence the packing density is relatively low and the electrons penetrate further into the target (Fig. 6b). More deeply channelled electrons have a lower probability of emission than those which interact near the surface and hence a component of the total BSE signal is modulated by the crystal structure of the target. Because the interaction between electrons and crystal structure depends on the angle of beam incidence, characteristic changes in BSE emission only occur whilst the incident beam is still well defined or collimated. As the beam diverges with penetration, the angular relationships between beam and crystal structure become more and more variable and eventually only a few electrons are travelling parallel to any given direction. The EC signal is therefore smeared-out over a uniform range rather than showing discrete intensities. Thus, most significant EC events occur close to the target surface, typically < 50 nm, although there is obviously some dependence on target atomic number. Divergent incident beams result in a similar

effect, even for near-surface events, such that it is essential to use a collimated beam with divergence angles of $< 10^{-3}$ rads.

The behaviour of an electron beam inside a crystalline target is best considered in terms of individual electrons. The motion of these electrons can be described as a superposition of plane or Bloch waves modulated by the periodic potential of the crystal structure. The waves are in fact solutions to the Schrödinger equation and physically represent the current flows inside the crystal structure. The relative contribution of each Bloch wave to the total EC signal varies according to the angle (θ) between the incident beam and the different planes of atoms in this structure, as predicted by the familiar Bragg relationship

$$n\lambda = 2d_{hkl}\sin\theta \qquad (4)$$

in which λ is the wavelength of the electrons (a constant determined by the accelerating voltage), d_{hkl} is the spacing between hkl atomic planes and n is the particular order of the reflection. In general, we can recognize two types of Bloch wave: Type I, which interacts weakly with the crystal structure,
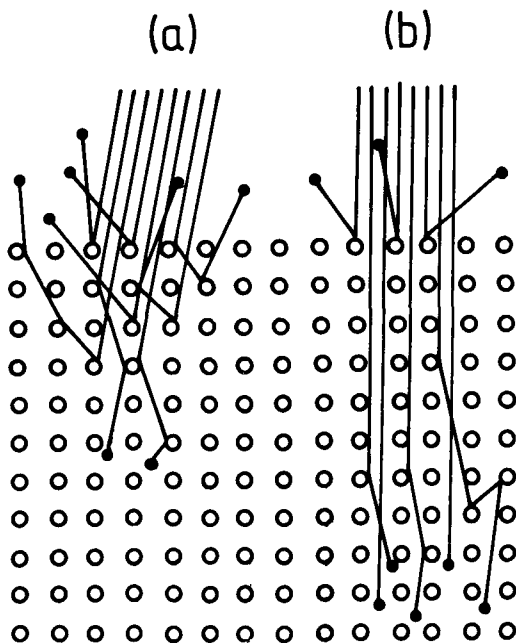
FIG. 6. Electron channelling effect. The variation in depth of electron penetration with angle of incidence relative to the target crystal structure results in either (a) near surface interactions and high BSE emission rates (Type II Bloch waves), or (b) deep penetration and low BSE emission rates (Type I Bloch waves). After Goldstein and Yakowitz (1975).
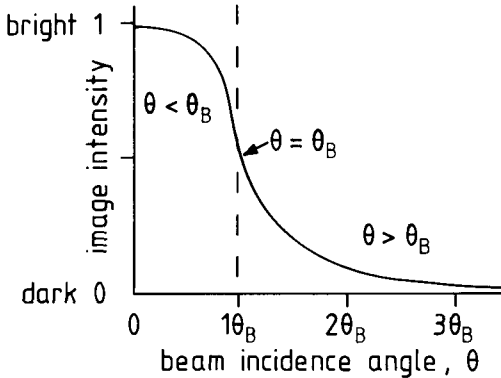
FIG. 7. Variation in emission intensity and hence image contrast for an individual Bloch wave as the angle of beam incidence (θ) passes through the Bragg angle (θ_B) for the target specimen. For Type II Bloch waves $\theta < \theta_B$; for Type I Bloch waves $\theta > \theta_B$. Modified from Joy (1974).

and Type II, which interacts strongly. The relative contribution of each type of wave depends on the relationships between θ and the Bragg angle (θ_B) of the target. This relationship is generalised in Fig. 7; note that as the incidence angle passes through θ_B the intensity of the BSE/EC signal is modulated. A number of models have been derived to explain this process quantitatively (e.g. Hirsch and Humphreys, 1970; Vicario et al., 1971; Spencer et al., 1974; Sandstrom et al., 1974) and each recognizes that many, rather than two, Bloch waves actually participate in the channelling process. Nevertheless, the fraction of primary electrons which reappear as BSE can still be calculated and the variation in the BSE/EC signal predicted for a particular set of crystal structure planes (e.g. Fig. 8).
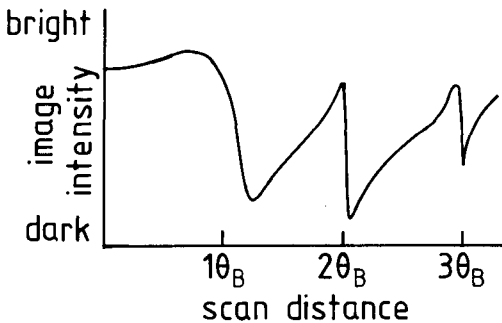

FIG. 8. Intensity profile of a typical electron channelling image along a single scan line in terms of the Bragg angle (θ_B). The intensity variations have been calculated from the sum of the first four Bloch waves. Modified from Joy (1974).

However, in practice all the different sets of planes present in the crystal structure of the target interact simultaneously with the electron beam to produce a composite electron channelling image, but the actual appearance of this image also depends on the target, the area scanned and beam collimation.

In normal SEM operation the incident beam is scanned in two directions across the target by the operation of two sets of deflection coils situated between the condenser and objective lenses. This scanning action causes the angle of beam incidence to change (by as much as 25°) over the region scanned, particularly at low magnifications and/or short working distances, and produces the exact conditions for electron channelling. If the target crystal structure remains constant over this region (Fig. 9a) the resulting image (Fig. 10a) is known
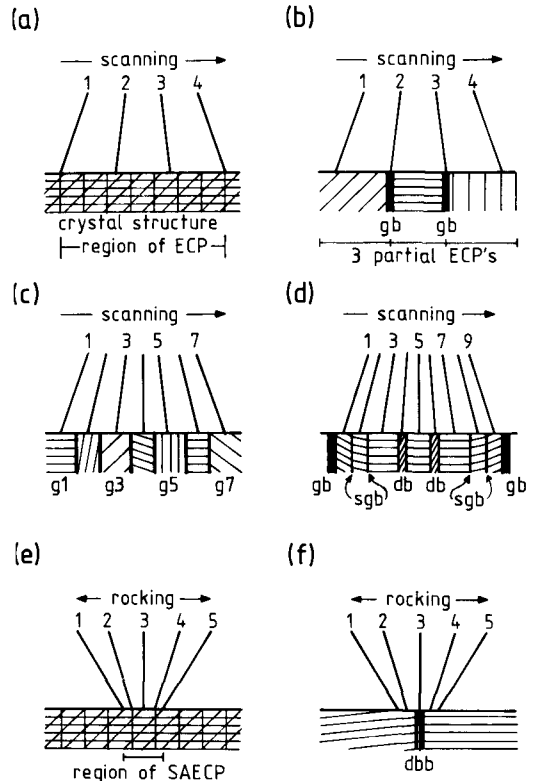
FIG. 9. Schematic formation of the different electron channelling images in terms of the relationship between the angle of incidence and the spatial resolution of the electron beam and the crystal structure of the target specimen. Notation as follows: g1, g2, g3, etc., grains 1–3 etc.; gb, grain boundary; sgb, subgrain boundary; db, deformation band; dbb, deformation band boundary. See text for details and also compare directly with Fig. 10.

as an electron channelling pattern (ECP) and is unique for the particular crystal structure of the area scanned (Coates, 1967; Booker et al., 1967). This can be verified by moving the target laterally which does not change the angular relationships between beam and target, provided the crystal structure remains constant, and hence the ECP stays the same. However, tilting the target does
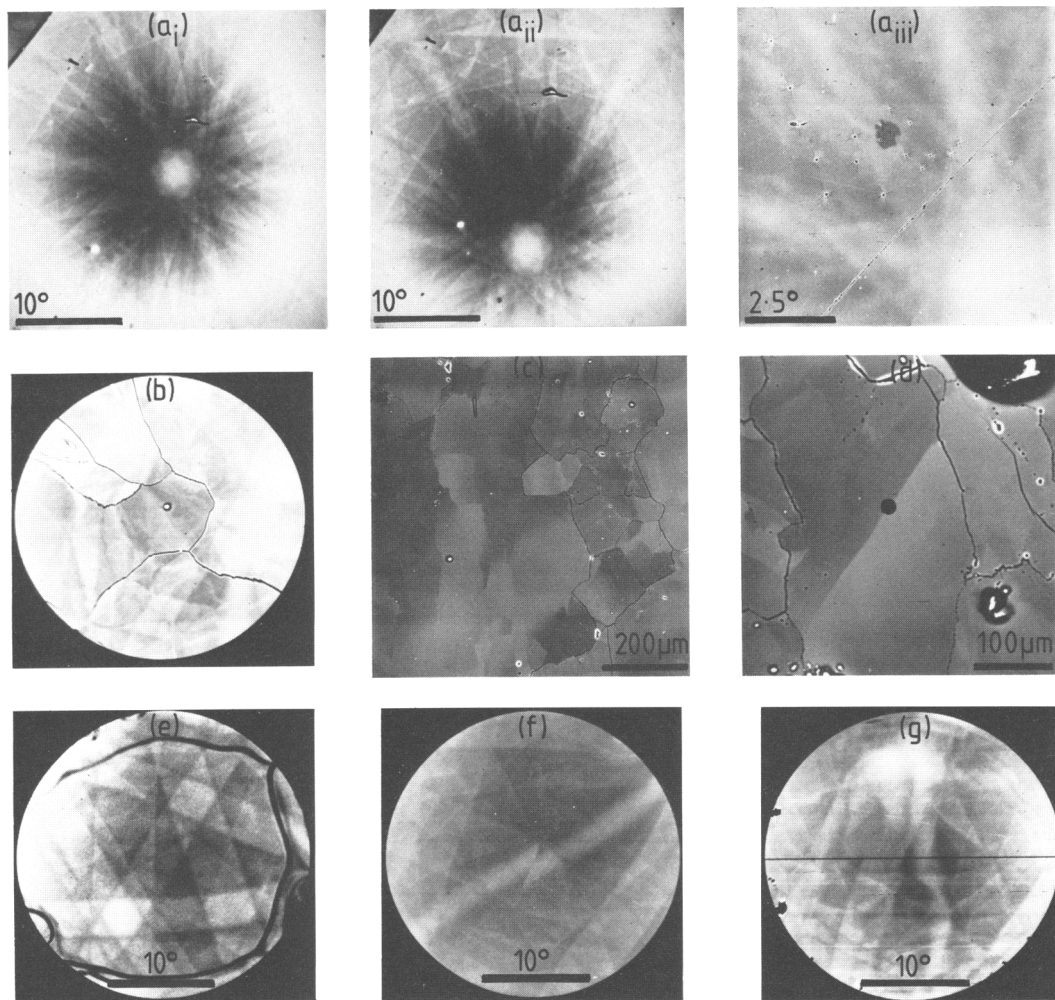

FIG. 10. Examples of the different types of electron channelling image. See text for details and also compare directly with Fig. 9. All specimens carbon-coated and imaged at 30 kV accelerating voltage. (a) Electron channelling patterns from quartz single crystals (patterns reveal orientations close to {0001}): (i)–(ii) show effect of tilting the target; (iii) shows the effect of increasing image magnification from $\sim 20 \times$ in the previous two images to $\sim 60 \times$ in this image (small crosses are the impressions of a Vickers pyramidal indenter—see Ferguson et al. in press). (b) Partial ECP from several adjacent grains in a quartzite (n.b. angular or spatial scales cannot be *accurately* determined in this type of image). (c) Orientation or crystallographic contrast image of grain and subgrain microstructure in a quartzite. (d) Orientation contrast image of an individual quartz grain showing contrast variations due to intragranular deformation; note particularly the sharp central boundary (see Fig. 10f). (e) Selected-area electron channelling pattern from an individual grain in a calcite vein (black lines are images of the grain boundaries). (f) SAECP from the region of the sharp deformation boundary indicated by the solid circle in Fig. 10d; note the displacement of the channelling lines/bands across the boundary which can be used to determine the type of boundary and mismatch across it. (g) Distorted SAECP from a quartz grain showing the effect of intense intragranular crystal plastic deformation (the horizontal black line is a reference orientation marked on the SAECP to aid pattern indexing—see Fig. 14).

change the angular relationships and consequently the ECP also changes (e.g. Fig. 10a_{ii}). For optimum contrast and detail in the ECP image the incidence angle should vary through at least 2θ_B, which is most likely at low magnifications and/or short working distances. As magnification (or working distance) increases, the scanning angle decreases and the proportion of the original ECP observed is reduced (Fig. 10a_{iii}). A similar effect is observed if the accelerating voltage is reduced. It is therefore advisable to image ECPs at relatively high accelerating voltages (e.g. 20–30 kV), short working distances (i.e. < 10 mm) and the lowest possible magnification (typically ∼ 20 times normal). In normal scanning operation, low magnification means that the electron beam traverses over a relatively large area of target (e.g. 2 × 2 mm), which may be unimportant for large, single-crystal specimens, but can lead to problems in polycrystalline targets with small grain size.

If a polycrystalline specimen is imaged under normal scanning conditions the angular relationship between incident beam and crystal structure varies from grain to grain, although the total scanning angle remains as before. The effective scanning angle for electron channelling consequently depends on the size of each grain (Fig. 9b) and each grain therefore contributes a reduced or partial ECP to the overall image (Fig. 10b). However, if the scanning angle remains effectively constant for each grain, but obviously varies between grains (Fig. 9c), then each grain provides a constant contrast to the image which is known as an orientation, crystallographic or electron channelling contrast image (Fig. 10c). This type of image remains susceptible to tilting since this changes the electron channelling conditions, but it is also susceptible to lateral shifts in position for exactly the same reason. Indeed, it is important to remember that even a slight shift in position can result in extreme changes in contrast of individual grains (e.g. from dark to bright). At high magnification (depending on grain size) orientation contrast images can be obtained from the internal structure of individual grains (such as subgrains etc.) because the subtle changes in crystal structure are still sufficient to cause the electron channelling conditions to vary (Fig. 9d and Fig. 10d).

We have seen that under normal scanning conditions the minimum area from which a useful ECP can be obtained is quite large and therefore restricts the application of ECP analysis. However, the resolution of ECPs can be considerably improved by modifying the SEM operating conditions. This is achieved by inserting a beam-defining aperture within the second condenser lens and by turning off the lower set of scan deflection coils, which together
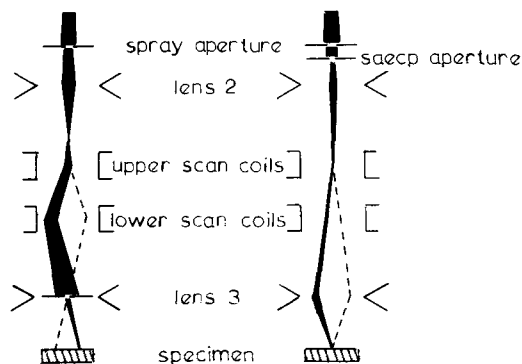

FIG. 11. Comparison between normal scanning (left) and selected-area diffraction (right) modes of SEM operation. See text for details.

move the crossover position of the electron beam from the objective lens to the surface of the target specimen (Fig. 11). Thus, rather than scanning over an area, the electron beam now 'rocks' about a fixed point on the target (van Essen and Schulson, 1969; van Essen et al., 1971). This rocking action produces the exact conditions for electron channelling (Fig. 9e), but the minimum area from which an ECP can be obtained now depends on how accurately the rocking position can be fixed and how much 'travel' there is about this position. Because the rocking position is chosen at will, this technique is also known as selected-area diffraction (SAD) and the ECPs (e.g. Fig. 10e) are referred to as selected-area electron channelling patterns (SAECP). In practice, the following operating steps are necessary to obtain the optimum SAD image (Fig. 12).

(1) Obtain a crystallographic image of the target using normal SEM conditions; focus this image at 'high' magnification (i.e. up to ∼ 500 ×) and move the chosen rocking position to the centre of the image (Fig. 12a).

(2) Switch to lowest magnification possible, insert the SAD aperture and turn off the lower scan-deflection coils; it is unlikely that the beam rocking position will be contained exactly within the plane of the target surface and so a distorted crystallographic contrast image of the target is most likely obtained (Fig. 12b).

(3) Adjust the objective lens so that the target surface coincides with the focal length of the upper deflection coils, which ensures that the rocking position is moved to the target surface; this has the effect of expanding the central part of the image to fill the CRT screen (i.e. improving the resolution by rocking closer and closer to a point on the target surface) until the crystallographic contrast image is replaced by a SAECP image, which is also
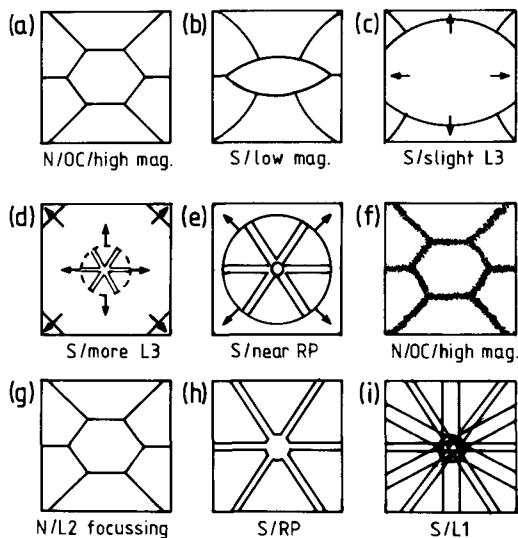
FIG. 12. Schematic representation of the formation of selected-area diffraction SEM electron channelling pattern images, with the following notation: N, normal scanning mode; S, selected-area diffraction mode; OC, orientation contrast image; mag., image magnification; L1–L3, operation of respectively the first and second condenser lenses and the objective lens; RP, 'rocking' position of electron beam. See text for further details.

expanded using the objective lens until the moment it too begins to break-up or exceeds the image field of view (Fig. 12c–e). This is the optimum rocking position.

(4) Switch on the lower deflection coils and return to 'high' magnification; due to the use of the objective lens to move the rocking position, the image will be out of focus (Fig. 12f) and must be refocused (Fig. 12g) using the second condenser lens. (Note: this action produces a small beam diameter but also a convergent beam and hence variable electron channelling conditions; beam convergence is overcome by operating the objective lens at much weaker currents than normal, which acts to collimate the beam.)

(5) Return to SAD conditions and readjust the objective lens to obtain the optimum conditions (Fig. 12h); in practice it is usually necessary to switch between SAD and normal operating conditions several times before the optimum SAECP is obtained (e.g. Fig. 10e).

(6) Contrast is added to the SAECP image by adjusting the first condenser lens in combination with applying black-level correction (Fig. 12i); in practice it is again usually necessary to make the adjustments to all three lenses in small amounts by switching between SAD and normal conditions.

It should be obvious from these operating conditions that it is a relatively simple matter to switch from SAECP image to crystallographic contrast image. Thus, any region of interest in a microstructural image can also be imaged via SAECP (Fig. 9f and Fig. 10 d and f). The minimum area of pattern formation in SAD is determined by aberrations in the objective lens, but is about ∼ 10 μm. Resolution can generally be improved by operating at shorter working distances (e.g. 5–10 mm), but significant improvements towards ∼ 1 μm resolution require 'dynamic focusing' in which the final lens is modulated in synchronism with the scanning system to overcome spherical aberrations (van Essen, 1971; van Essen et al., 1971); a process also known as 'spiral scanning' (Hall and Skinner, 1978). Eventually, however, the maximum SAECP resolution may still exceed the scale of deformation induced into the crystal microstructure, resulting in imperfect ECPs. If this deformation occurred under low homologous temperatures the ECP will show a loss of fine detail, a uniform broadening of channelling bands and a reduction in contrast relative to the background, but all lines/bands will remain straight. Deformation at high homologous temperatures has similar effects, but also leads to a distortion of the channelling bands (i.e. bending and irregular band-widths) due to the polygonisation of the crystal structure and the development of subcells with slightly different rotation vectors (e.g. Fig. 10g). Deterioration of ECP images (similar to the effects of low-temperature deformation) can also be due to the poor condition of the specimen surface. This is usually caused by the effects of mechanical polishing necessary to produce flat, polished surfaces. Thus very careful specimen preparation is necessary for successful electron channelling analysis.

Specimen preparation for BSE analysis

One of the most attractive features of secondary electron SEM analysis is that very little specimen preparation is usually necessary. However, due to the different origins of the various BSE signals specimen preparation becomes an important consideration and, unless there is a particular requirement to image the topographic characteristics of BSE emission, specimens intended for BSE analysis should be polished as flat as possible. Suggestions in the literature (e.g. Krinsley et al., 1983; Pye and Krinsley, 1983) that slight surface topography is useful in fine grained specimens are misleading; although general image quality and resolution may be improved this is always at the expense of BSE signal resolution and only where there is no variation in the BSE signal (e.g. in monomineralic

specimens) is topography likely to be useful (i.e. to reveal grain boundaries etc.). Surface topography is most easily removed by conventional polishing techniques used in the preparation of optical thin-sections or electron microprobe samples, although depending on the nature of the specimen (i.e. coarse or fine grained) polishing with finer grade abrasives or pastes than normally used may be required (e.g. slates often need polishing down to 0.25 μm diamond paste). Unfortunately, polishing with abrasives is mechanical and introduces sufficient damage into the surface (i.e. crystal structure) layers of a specimen to completely eliminate electron channelling effects. It therefore follows that conventional polishing techniques are only suitable for BSE Z-contrast analysis. The mechanical damage introduced by abrasives can be removed using a chemical–mechanical polishing technique involving an alkaline silica-sol slurry and a polyurethane-foam substrate (Fynn and Powell, 1979; see also Lloyd, 1985). This polishing process results in very slow abrasion rates (e.g. 1–2 μm/hr or $\sim$ 1 atomic monolayer per second) and introduces negligible damage whilst removing earlier damage. After polishing is complete it is important to thoroughly clean the specimen surface and to leave it free from any contamination (especially hydrocarbon products) which may breakdown under the influence of the electron beam and deposit debris. Specimens should therefore be rinsed in cold water and then a solvent (e.g. ethanol) and finally dried using a hot-air dryer. They should also be stored in a clean, dry place and it is recommended that after storage an inert gas aerosol spray is used to remove any stray dust particles.

Specimens are examined in the SEM under conditions of high vacuum. Excess electrons therefore accumulate on the surface of non-conducting specimens (i.e. most rocks and minerals) as a 'space-charge' region with negative potential, causing irregular deflections of the incident electron beam on successive scans. CRT images may also appear very bright and/or 'flicker' intermittently between very bright and dark. Specimen charging is prevented by depositing a thin layer of a conducting material on to the specimen surface using high-temperature vacuum evaporation or plasma discharge techniques (Pfeffercorn, 1973; Echlin, 1974). However, whereas secondary-electron emission and resolution are improved by using a coating material of high atomic number such as gold (Everhart, 1970), such materials form energy barriers to both electron penetration and BSE emission and hence degrade any BSE image. It is therefore necessary to use a material with a low atomic number, such as carbon, but since electron channelling effects originate from very close to the specimen surface (typically < 50 nm) the thickness of carbon deposited must be carefully monitored for BSE electron channelling analysis. Lloyd et al. (1981) determined that 7–15 nm of carbon layer is sufficient to prevent specimen charging and yet does not degrade the electron channelling signal.

An alternative method of charge prevention should also be mentioned, namely the 'environmental cell' (Robinson and Robinson, 1978; Robinson and Nickel, 1979). This approach maintains the specimen at a much lower vacuum which it is hoped will help conduct charge away from the surface. As such, the environment cell should be particularly useful in the examination of gassy or friable specimens which are likely to contaminate high vacuums.

Applications of SEM/BSE signals

Atomic number or Z-contrast

Z-contrast images (e.g. Figs. 1a and 3a) are perhaps the easiest SEM/BSE image to obtain. Indeed, this type of image has been available with the electron microprobe for many years (Kimoto and Hashimoto, 1966), although the electron optical and BSE detection systems present in these instruments are generally inferior to those in SEMs. Compared with the optical microscope, the SEM offers considerably superior image resolution and has the added advantage of immediate quantitative X-ray microanalysis of Z-contrast images. However, mineral polymorphs (such as the andalusite-sillimanite-kyanite system) do present a problem since their $\bar{Z}$ and hence $\bar{\eta}$ values and image contrasts are identical. Therefore, when imaging polymorphic minerals using SEM Z-contrast, other characteristics (e.g. form etc.) will generally have to be relied upon to distinguish the different varieties. Alternatively, since direct comparison between SEM and optical micrographs is also possible using uncovered thin-sections, this approach can be used to identify mineral polymorphs. The fact that Z-contrast images have a familiar appearance should make for rapid acceptance of the technique as well as facilitating interpretation and comparison of the images. These advantages of SEM Z-contrast analysis make for a wide range of possible applications; in fact the technique can be used whenever and wherever the optical microscope is considered. For this reason, no particular examples of Z-contrast analysis are described in this review, rather the interested reader is referred to the following recent publications: Robinson and Robinson (1978); Hudson et al. (1978); Robinson and Nickel (1979); Ferguson et al. (1980); Ball and McCarthney (1981); Hall and Lloyd (1981); Hall and Skinner (1981); Lloyd and Hall (1981); Krinsley et al. (1983); Pye and Krinsley (1983,

1984); Pye (1984); White *et al.* (1984, 1985) and Lloyd (1985).

Electron channelling contrast

SEM electron channelling contrast analysis is more difficult to perform than Z-contrast analysis due to the need for additional (usually non-standard) attachments in the electron-optical system and stricter specimen preparation demands. Similarly, the interpretation of electron channelling images is also more involved. As we saw above, electron channelling originates from within the structure of crystalline materials and is responsible for two distinct SEM images: orientation contrast (e.g. Fig. 1*b*) and electron channelling patterns (Fig. 1*c*), with ECPs being used to index the regions observed via orientation contrast. Electron channelling analysis can be performed on solid specimens several centimetres in size and consequently the technique represents a potentially unique opportunity for geological research, particularly in crystal fabrics, since it overcomes deficiencies associated with other methods (e.g. universal-stage optical microscopy, X-ray texture goniometry and transmission electron microscopy). However, this potential has only recently been recognized (Saimoto *et al.*, 1980; Hall and Lloyd, 1980; Lloyd and Hall, 1981; Lloyd *et al.*, 1981) and actual applications are therefore rare (e.g. Christiansen, 1986; Lloyd and Ferguson, 1986; Lloyd *et al.*, in press; Ferguson *et al.*, in press). The rest of this section concentrates on the ancillary expertise necessary to interpret electron channelling images, although, because orientation contrast images are similar in appearance to some polarised light micrographs (e.g. consider Fig. 1*b*), their use and interpretation should be reasonably straightforward. Unfortunately, contrast difference in no way represents a specific misorientation. The maximum resolution possible in orientation contrast images is still superior to that obtained with the optical microscope and the misorientation indicated is also better (Lloyd and Ferguson, 1986). The interpretation of ECPs is an altogether different matter.

The appearance of any ECP is determined by the angular relationship between the electron beam and the crystal structure at the point of incidence. It therefore follows that the range of patterns observed is a function of crystal symmetry since the periodicity of crystal structure results in a continuous, but eventually repeated, variation in ECP configuration. This leads to the recognition of 'ECP-maps' (Joy *et al.*, 1971) which extend over the whole of the crystallographic stereogram or unit triangle required by symmetry to include all possible orientations and ECP configurations. The map area is a minimum for cubic symmetry classes and increases as symmetry decreases. ECP-maps are constructed by gradually tilting and rotating a crystal about a fixed point of beam incidence and photographically recording the individual patterns observed after every few degrees of tilt/rotation (see Lloyd, 1985; and Lloyd and Ferguson, 1986, for details). The patterns are then merged together into a complete map, but to minimise spherical distortions inherent in the recording process it is recommended that maps are constructed over a spherical surface (Stott *et al.*, 1975). These 'spherical ECP-maps' (e.g. Fig. 13) also facilitate indexing of ECPs and representation of ECP data, as follows.

Accurate and meaningful indexing and representation of ECPs not only involves the availability of the relevant spherical ECP-map, but also requires that the crystallographic and specimen coordinate systems can be related to each other. This means that, in general, oriented specimens should be used. The first step necessary in relating crystallographic and specimen coordinates is to ensure that the specimen surface (which it is assumed has been prepared to include two of the three specimen coordinate directions) is perpendicular to the electron beam (assuming normal incidence). The normal to the specimen surface (N) is therefore also the normal to any ECP obtained from this surface. Probably the best method of ensuring this configuration involves fixing a small piece of {111} silicon-slice to the specimen surface. The {111} ECP for silicon is very distinctive and for normal beam incidence should be symmetrical about the centre of the pattern. The tilt control can be used to obtain the correct appearance. The next step is to define the rotation of the specimen about N. This requires that one of the specimen coordinate axes (e.g. a mineral lineation) within the specimen surface can be recognized and hence its direction (R) in the SEM/OC image can be determined. However, because a rotation about N exists between OC and SAD images (van Essen and Verhoeven, 1974; Davidson, 1976), it is necessary to define R for both images. This is achieved by firstly aligning R either vertically or horizontally in the OC image. On switching to SAD the specimen image disappears and is replaced by a SAECP which contains no indication of R. But, if the SAECP image is defocused (i.e. steps *b*–*g* in Fig. 12 are reversed), a 'blurred' OC image is produced in which R can be recognized, although it will not be vertical/horizontal. R can be re-aligned via the rotation control and, because this rotation occurs about N, refocusing the SAECP image has no effect on the new alignment and R will therefore be vertical/horizontal on all SAECPs obtained from the specimen. Obviously, R is no longer vertical/horizontal in OC images, but its new direction can be easily observed.
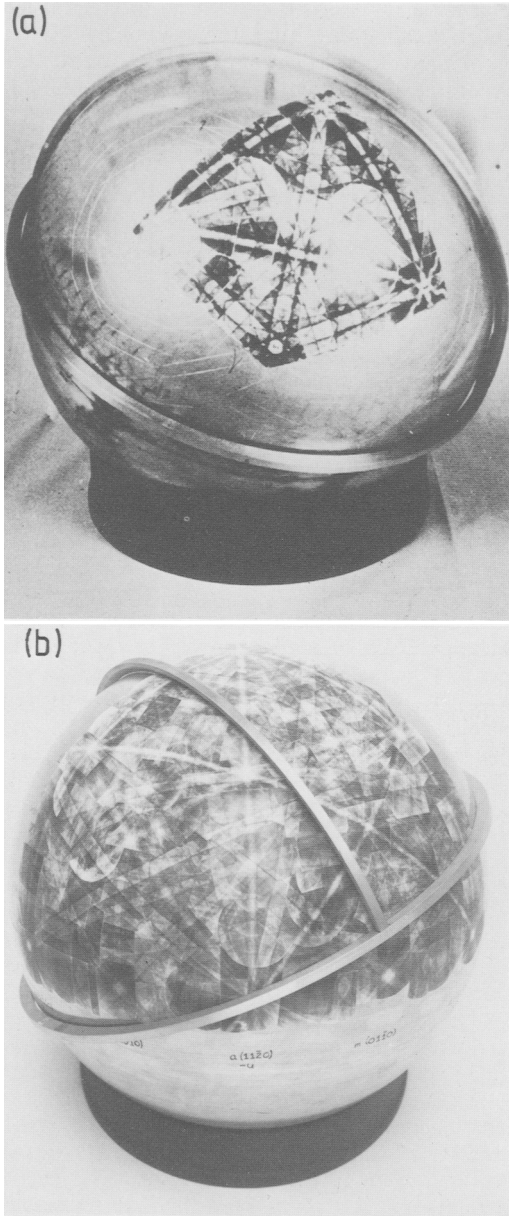
FIG. 13. Examples of spherical ECP-maps constructed from single crystals of (a) copper (face-centred cubic symmetry) and (b) quartz (trigonal symmetry).

specimen and crystallographic coordinate systems are generally recognized (e.g. Hatherley and Hutchinson, 1979):

(1) inverse pole figure, in which a particular specimen direction (e.g. N) is plotted in crystallographic coordinates;

(2) pole figure, in which a particular crystallographic axis is plotted in specimen coordinates;

(3) orientation distribution function (ODF) diagram which represents a complete but complex relationship between specimen and crystallographic coordinate systems.

These three relationships are shown in Fig. 14 for a general crystallographic coordinate system defined by its ECP-map (xyz) and an orthogonal specimen coordinate system (NRP). Assuming that the specimen has been oriented as described above, the centre of any ECP represents the ECP/specimen normal direction N. This position of N within the ECP-map is determined by visual comparison, but can be accurately fixed by means of great-circle rulers graduated in degrees (e.g. Fig. 13b). These rulers are used to measure spherical angles which relate (xyz) to (NRP). For the inverse pole figure only the position of N in terms of (xyz) is required and this is easily obtained via the spherical angles θ and φ (Fig. 14a). However, rotation about N is not recognized. The pole figure recognizes this rotation by relating a specific crystallographic direction (i.e. x, y, z etc.) to the specimen directions N and R (Fig. 14b), although a different pair of spherical angles θ_{xyz}, φ_{xyz} is required for each crystallographic direction. The ODF relates (xyz) to (NRP) exactly via only three spherical angles θ, φ, ψ (Fig. 14c), but interpretation of the data derived from this approach awaits further investigation (Lloyd et al., in prep.).

As mentioned previously, applications of SEM electron channelling in the geological sciences have been limited, but the technique has been used successfully in metallurgy and materials science for several years (for example, see reviews by Hall and Hutchinson, 1980; Hall, 1981; Joy and Newbury, 1977; and Joy et al., 1982). The most obvious geological applications are probably in studies of microstructures and crystal fabrics due to natural deformations; see Table 1 for a general summary of the applications to date. However, the number of individual ECPs needed for statistically meaningful crystal fabric analysis (i.e. ~ 500) does make the technique somewhat laborious, but the effort is rewarded by the absolute discriminatory nature of the technique which ensures that crystal (i.e. ECP images) and microstructural (i.e. orientation contrast images) data are maintained in an exact one-to-one correspondence. This ability is claimed
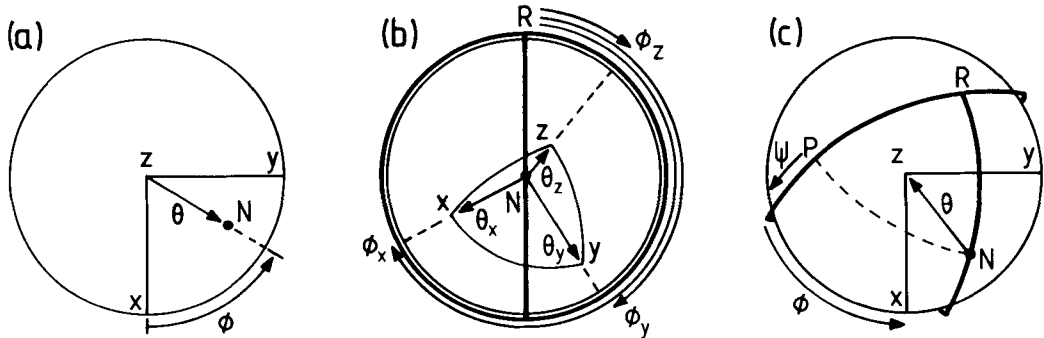
The specimen is now accurately oriented within the SEM and the relationship between specimen and crystallographic coordinate systems can be established for each ECP via the spherical ECP-map.

In fact, three different relationships between

FIG. 14. Determination of (a) inverse pole figure, (b) pole figure, and (c) orientation distribution function diagrams using SAECPs and spherical ECP-maps, with the following notation: NRP, specimen coordinate system (N, direction normal to specimen surface *and also the SAECPs*; R, a reference direction in the plane of the specimen surface and marked on each SAECP—see for example Fig. 10g; P, the mutual perpendicular direction); *xyz*, generalized crystal structure coordinate system; θ, spherical angles measured either towards (a) or from (b and c) N; φ, spherical angles measured in either the primitive plane of the ECP-map (a and c) or the plane of the specimen surface (b); ψ, spherical angles measured in the plane of the specimen surface from the direction P.

Table 1. Summary of possible applications of electron channelling techniques in the geological sciences and in general

Application	Geology	General
microstructural analysis	Lloyd & Hall 1981 Lloyd et al. 1981 Christiansen 1986 Lloyd & Ferguson 1986 Lloyd et al. in prep.	Nakagawa 1986
crystal fabric determination	Lloyd et al. in press Lloyd et al. in prep.	Lloyd 1985
crystal plastic deformation and/ or misorientation determination	Saimoto et al. 1980 Christiansen 1986 Lloyd & Ferguson 1986	Schulson 1971 Stickler et al. 1971 Joy et al. 1972 Spencer et al. 1974 Davidson 1974, 1977, 1982 Newbury & Yakowitz 1975 Crompton & Martin 1980 Yakowitz 1974
analysis of microfracturing	Lloyd et al. 1981 Ferguson et al. in press	Davidson 1974, 1977, 1982 Tchorzewski & Hutchinson 1978 Prince & Martin 1979 Lankford & Davidson 1982
lattice parameter determination		Joy 1974

by no other fabric analysis technique or methodology. On a more localized level, the orientation mismatch between grains or internal regions of individual grains can be determined using electron channelling with an accuracy of better than 1° (e.g. Fig. 10f), whilst the deterioration in ECP image with plastic deformation (e.g. Fig. 10g) may provide a means of estimating actual strain magnitudes in

crystal structures (see, for example, Yakowitz, 1974, p. 473 and appendix).

Conclusions

In this contribution I have reviewed the use of SEM backscattered electron techniques in the geological sciences. Three different types of image

can be obtained: atomic number contrast (Z-contrast), images based on variations in composition; orientation contrast, images based on changes in crystal structure; and electron channelling patterns, distinct configurations of lines and bands of different contrasts which are unique for a particular crystal structure (orientation). Both orientation contrast and electron channelling patterns result from the 'channelling' of the incident electrons through the crystal structure of a target specimen. The incorporation of conventional X-ray microanalytical facilities into the SEM augments the various BSE signals by providing immediate quantitative compositional determination. Together, these techniques provide a unique opportunity to investigate the microstructure of geological specimens on a scale and with a resolution hitherto unknown. The BSE signals and images are generally simple to understand and obtain provided certain specimen preparation procedures are followed, although ECP analysis does require additional SEM hardware and extra facilities for interpretation of images. The very novelty of these BSE techniques means that geological applications have so far been rare and largely restricted to Z-contrast images. However, now that a new generation of SEMs is available with full BSE and electron channelling facilities, plus the fact that the methodology for accurate interpretation of ECPs has recently been developed, the geological usage of Z-contrast, orientation contrast and ECP images should rapidly increase.

Acknowledgements

References

Ball, M. D., and McCarthney, D. G. (1981) *J. Microsc.* **24**, 57–68.

Bishop, H. E. (1966) *Fourth Cong. Int. X-ray Opt. Microsc. (Orsay).* Hermann, Paris, 153–8.

——(1974) In *Quantitative Scanning Electron Microscopy* (D. B. Holt, M. D. Muir, P. R. Grant, and I. M. Boswarva, eds.). Academic Press, New York, 41–64.

Booker, G. R., Shaw, A. M. B., Whelan, M. J., and Hirsch, P. B. (1967) *Philos. Mag.* **16**, 1185–91.

Christiansen, F. G. (1986) *Tectonophys.* **121**, 175–96.

Coates, D. G. (1967) *Philos. Mag.* **16**, 1179–84.

Cosslett, V. E., and Thomas, R. N. (1965) *Brit. J. Appl. Phys.* **16**, 779–96.

Crompton, J. S., and Martin, J. W. (1980) *Metallography*, **13**, 225–34.

Davidson, D. L. (1974) *Proc. 7th Ann. SEM Symp.*, IITRI, Chicago, 927–34.

——(1976) *J. Phys.* **E9**, 341–3.

——(1977) *Proc. 10th Ann. SEM Symp.*, IITRI, Chicago, 431–6.

——(1982) *J. Mater. Sci. Lett.* **1**, 236–8.

Duncumb, P., and Shields, P. K. (1963) *Brit. J. Appl. Phys.* **14**, 617.

Echlin, P. (1974) *Proc. 7th Ann. SEM Symp.*, IITRI, Chicago, 1019.

Everhart, T. E. (1970) *Proc. 3rd Stereoscan Colloquium*, Morton Grove, Illinois, Kent–Cambridge Scientific, 1.

——and Thornley, R. F. M. (1960) *J. Sci. Instrum.* **37**, 246–8.

Ferguson, C. C., Harvey, P. K., and Lloyd, G. E. (1980) *Contrib. Mineral. Petrol.* **75**, 339–52.

——Lloyd, G. E., and Knipe, R. J. (in press). *Can. J. Earth Sci.*

Fynn, G. W., and Powell, W. J. A. (1979) *The Cutting and Polishing of Electro-Optic Materials.* Adam Hilger Ltd., London.

Goldstein, J. I., and Yakowitz, H. (1975) *Practical Scanning Electron Microscopy.* Plenum, New York.

——Newbury, D. E., Echlin, P., Joyce, D. C., Fiori, C., and Lifshin, E. (1981) *Scanning Electron Microscopy and X-ray Microanalysis.* Plenum, New York.

Hall, M. G. (1981) *Proc. 14th Ann. SEM Symp.* IITRI, Chicago, 409–22.

——and Hutchinson, W. B. (1980) *Metall. Mater. Technol.* **12**, 371–5.

——and Lloyd, G. E. (1980) *Can. Mineral.* **18**, 559–61.

————(1981) *Am. Mineral.* **66**, 362–8.

————(1983) Ibid. **68**, 843–5.

——and Skinner, G. K. (1978) *J. Phys.* **E11**, 1129–32.

————(1981) *J. Microsc.* **124**, 69–75.

Hatherley, M., and Hutchinson, W. B. (1979) *Inst. Metall. (London) Monog.* 5.

Heinrich, K. J. F. (1964) *Adv. X-ray Anal.* **7**, 325–39.

——(1966) *Fourth Cong. Int. X-ray Opt. Microsc. (Orsay)*, Hermann, Paris, 159.

Hirsch, P. B., Howie, A., and Whelan, M. J. (1962) *Philos. Mag.* **7**, 2095–100.

——and Humphreys, C. J. (1970) *Proc. 3rd Ann. SEM Symp.*, IITRI, Chicago, 449–55.

Hudson, D. R., Robinson, B. W., and Vigers, R. B. W. (1978) *Can. Mineral.* **64**, 121–6.

Joy, D. C. (1974) In *Quantitative Scanning Electron Microscopy* (D. B. Holt, M. D. Muir, P. R. Grant, and I. M. Boswarva, eds.). Academic Press, New York.

——Booker, G. R., Fearon, E. O., and Bevis, M. (1971) *Proc. 4th Ann. SEM Symp.*, IITRI, Chicago, 497–504.

Joy, D. C., and Newbury, D. E. (1977) *Proc. 10th Ann. SEM Symp.*, IITRI, Chicago, 445–54.

———— and Davidson, D. L. (1982) *J. App. Phys.* **53,** R81–122.

———— and Hazzledine, P. M. (1972) *Proc. 5th Ann. SEM Symp.*, IITRI, Chicago, 97–103.

Kimoto, S., and Hashimoto, H. (1966) In *The Electron Microprobe* (T. D. McKinley, K. F. J. Heinrich, and D. B. Wittry, eds.).

Krinsley, D. H., Pye, K., and Kearsley, A. T. (1983) *Geol. Mag.* **120,** 109–14.

Lankford, J., and Davidson, D. L. (1982) *J. Mater. Sci.* **17,** 1501–7.

Lin, P. S. D., and Becker, R. P. (1975) *Proc. 8th Ann. SEM Symp.*, IITRI, Chicago, 61–70.

Lloyd, G. E. (1985) Mineral. Assoc. Can. Short Course 11: *Applications of Electron Microscopy in the Earth Sciences* (J. C. White, ed.), 151–88.

—— and Ferguson, C. C. (1986) *J. Struct. Geol.* **8,** 517–26.

—— and Hall, M. G. (1981) *Tectonophys.* **78,** 687–98.

————Cockayne, B., and Jones, D. W. (1981) *Can. Mineral.* **19,** 505–18.

——Ferguson, C. C., and Law, R. D. *Tectonophys.* (in press).

Nakagawa, S. (1986) *Jeol. News* **24E,** 7–14.

Newbury, D. E. (1975) *Proc. 8th Ann. SEM. Symp.*, IITRI, Chicago.

Niedrig, H. (1978) *Scanning* **1,** 17–34.

Oatley, C. W. (1972) *The Scanning Electron Microscope.* Cambridge University Press.

Pfeffercorn, G. E. (1973) *Proc. 6th Ann. SEM Symp.*, IITRI, Chicago, 751.

Prince, K. C., and Martin, J. W. (1979) *Acta Metall.* **27,** 1401–8.

Pye, K. (1984) *Geol. Mag.* **121,** 81–4.

——Krinsley, D. (1983) *Nature,* **301,** 412–13.

————(1984) *J. Sed. Petrol.* **54,** 877–88.

Robinson, B. W., and Nickel, E. G. (1979) *Am. Mineral.* **64,** 1322–8.

————(1983) Ibid. **68,** 840–2.

Robinson, V. N. E. (1973) *J. Phys.* **D6,** L105–7.

——(1975) *Proc. 8th Ann. SEM Symp.*, IITRI, Chicago, 51–60.

——and Robinson, B. W. (1978) *Proc. 11th Ann. SEM Symp.*, IITRI, Chicago, 595–602.

Saimoto, S., Helmstaedt, H., Kempson, D., and Schulson, E. M. (1980). *Can. Mineral.* **18,** 251–9.

Sandstrom, R., Spencer, J. P., and Humphreys, C. J. (1974) *J. Appl. Phys.* **D7,** 1030–46.

Schulson, E. M. (1971) *J. Mater. Sci.* **12,** 1071–87.

Schur, K., Blashke, R., and Pfeffercorn, G. E. (1974) *Proc. 7th Ann. SEM Symp.*, IITRI, Chicago, 1003–10.

Shimuzu, R., and Murata, K. (1971) *Optik (Stuttgart),* **36,** 59–65.

Spencer, J. P., Booker, G. R., Humphreys, C. J., and Joy, D. C. (1974) *Proc. 7th Ann. SEM Symp.* IITRI, Chicago, 919–26.

Stephen, J., Smith, B. J., Marshall, D. C., and Witham, E. M. (1975) *J. Phys.* **E8,** 607–18.

Stickler, R., Hughes, C. W., and Booker, G. R. (1971) *Proc. 4th Ann. SEM Symp.*, IITRI, Chicago, 473–83.

Stott, D. E., Wise, M. L. H., and Hutchinson, W. B. (1975) *J. Microsc.* **105,** 305–7.

Tchorzewski, R. M., and Hutchinson, W. B. (1978) *Met. Trans.* **9A,** 1113–24.

van Essen, C. G. (1971) *Proc. 25th Ann. Meet. EMAG, Cambridge.* Inst. Phys., London.

——and Schulson, E. M. (1969) *J. Mater. Sci.* **4,** 336–9.

——and Verhoeven, J. D. (1974) *J. Phys.* **E7,** 768–9.

——Schulson, E. M., and Donaghy, R. H. (1971) *J. Mater. Sci.* **6,** 213–17.

Vicario, E., Pitaval, M., and Fontaine, G. (1971) *Acta Crystallogr.* **A27,** 1.

Wells, O. C. (1970) *Appl. Phys. Letters,* **16,** 151–3.

——(1974) *Scanning Electron Microscopy* McGraw-Hill, New York.

White, S. H., Shaw, H. F., and Huggett, J. M. (1984) *J. Sed. Petrol.* **54,** 487–94.

——Huggett, J. M., and Shaw, H. F. (1985) *Mineral. Mag.* **49,** 413–23.

Wolf, E. D., and Everhart, T. E. (1969) *Proc. 2nd Ann. SEM Symp.*, IITRI, Chicago, 43–4.

Yakowitz, H. (1974) In *Quantitative Scanning Electron Microscopy* (D. B. Holt, M. D. Muir, P. R. Grant, and I. M. Boswarva, eds.). Academic Press, New York.

APPENDIX

BASIC   program   to   calculate   mean   atomic   number   and   mean
backscattered electron coefficient of minerals from their formulae

```
1 PRINT"              MEATNO"
2 PRINT:PRINT:PRINT
3 PRINT"PROGRAM TO CALCULATE MEAN ATOMIC NUMBER"
4 PRINT"     AND MEAN BACKSCATTERED ELECTRON"
5 PRINT"          COEFFICIENT OF MINERALS     "
7 PRINT:PRINT:PRINT
19 REM ***************************************
20 REM ***    INPUT CONSTANTS AND DIMENSIONS    ***
21 REM ***************************************
25 DIM C(20),A$(100),Z(100),NU(100),Z1(20),Z2(30)
26 DIM W1(20),B$(20)
27 M=0:N2=0:M1=0:N3=0
29 REM ***************************************
30 REM ***    READ ELEMENT SYMBOLS A$, ATOMIC   ***
31 REM *** WEIGHTS Z, AND BSE COEFFICIENTS NU ***
32 REM ***************************************
35 FOR I=1 TO 92:READ A$(I):NEXT I
45 FOR I=1 TO 92:READ Z(I):NEXT I
55 FOR I=1 TO 92:READ NU(I):NEXT I
97 REM ***************************************
98 REM ***        CALCULATION SUBROUTINE      ***
99 REM ***************************************
105 PRINT"NO. OF ELEMENTS IN FORMULA ?":INPUT E
120 FOR I=1 TO E
125 PRINT "SYMBOL AND NO. ATOMS OF ELEMENT NO.";I
130 INPUT B$(I),Z2(I)
135 NEXT I
140 FOR J=1 TO E
145 FOR I=1 TO 92
147 IF B$(J)<>A$(I) THEN GOTO 160
150 W1(J)=Z(I)*Z2(J)
155 M=M+W1(J):C(J)=NU(I):Z1(J)=I
160 NEXT I
165 NEXT J
175 FOR J=1 TO E
183 M1=M1+(W1(J)*Z1(J)/M)
185 N1=W1(J)*C(J)/M:N2=N2+N1
195 NEXT J
197 PRINT:PRINT:PRINT
198 PRINT "MINERAL",
200 FOR J=1 TO E
210 PRINT B$(J);Z2(J);
215 NEXT J
216 PRINT:PRINT
219 PRINT "MEAN ATOMIC NUMBER: ";M1
220 PRINT "BSE COEFFICIENT   : ";N2
267 PRINT:PRINT:PRINT
990 STOP
994 REM ***************************************
995 REM ***        DATA STATEMENTS        ***
996 REM ***                               ***
997 REM ***        ELEMENT SYMBOLS        ***
998 REM ***************************************
1000 DATA "H","HE","LI","BE","B","C","N","O","F"
1001 DATA "NE","NA","MG","AL","SI","P","S","CL"
1002 DATA "AR","K","CA","SC","TI","V","CR","MN"
1003 DATA "FE","CO","NI","CU","ZN","GA","GE","AS"
1004 DATA "SE","BR","KR","RB","SR","Y","ZR","NB"
1005 DATA "MO","TC","RU","RH","PD","AG","CD","IN"
1006 DATA "SN","SB","TE","I","XE","CS","BA","LA"
1007 DATA "CE","PR","ND","PM","SM","EU","GD","TB"
1008 DATA "DY","HO","ER","TM","YB","LU","HF","TA"
1009 DATA "W","RE","OS","IR","PT","AU","HG","TL"
1010 DATA "PB","BI","PO","AT","RN","FR","RA","AC"
1011 DATA "TH","PA","U"
2000 REM ***************************************
2001 REM ***        DATA STATEMENTS        ***
2002 REM ***                               ***
2003 REM ***    ELEMENT ATOMIC WEIGHTS     ***
2004 REM ***************************************
2005 DATA 1.008,4.003,6.939,9.012,10.81,12.011
2006 DATA 14.007,15.999,18.998,20.183,22.991
2007 DATA 24.312,26.982,28.086,30.974,32.064
2008 DATA 35.453,39.948,39.102,40.08,44.956,47.9
2009 DATA 50.942,51.996,54.938,55.847,58.933
2010 DATA 58.71,63.54,65.37,69.72,72.59,74.922
2011 DATA 78.96,79.909,83.8,85.47,87.62,88.905
2012 DATA 91.22,92.906,95.94,99,101.9,102.905
2013 DATA 106.4,107.87,112.4,114.82,118.69,121.75
2014 DATA 127.6,126.904,131.3,132.905,137.34
2015 DATA 138.91,140.12,140.907,144.24,147,150.35
2016 DATA 151.96,157.25,158.924,162.5,164.93
2017 DATA 167.26,168.934,173.04,174.97,178.49
2018 DATA 180.948,183.85,186.2,190.2,192.2,195.09
2019 DATA 196.967,200.59,204.37,207.19,208.98,209
2020 DATA 210,222,223,226,227,232.038,231,238.03
3000 REM ***************************************
3001 REM ***        DATA STATEMENTS        ***
3002 REM ***                               ***
3003 REM ***   ELEMENT BSE COEFFICIENTS    ***
3004 REM ***************************************
3005 DATA .01,.021,.031,.043,.054,.066,.079,.093
3006 DATA .107,.121,.136,.15,.164,.176,.189,.201
3007 DATA .212,.223,.233,.243,.253,.263,.273,.282
3008 DATA .291,.3,.309,.317,.325,.332,.339,.345
3009 DATA .35,.355,.36,.365,.37,.375,.379,.384
3010 DATA .388,.392,.396,.4,.404,.408,.412,.415
3011 DATA .419,.423,.426,.43,.433,.436,.439,.443
3012 DATA .446,.449,.452,.455,.458,.461,.463,.466
3013 DATA .469,.472,.474,.477,.479,.482,.485,.487
3014 DATA .490,.492,.495,.498,.501,.504,.507,.509
3015 DATA .510,.512,.513,.515,.516,.517,.518,.519
3016 DATA .520,.521,.522,.523
```